Available online at www.sciencedirect.com
SCIENCE DIRECT®
Journal of Chromatography A, 1092 (2005) 2–16
JOURNAL OF CHROMATOGRAPHY A
www.elsevier.com/locate/chroma

Optimizing control of simulated moving beds—experimental implementation

Stefanie Abel[a], Gültekin Erdem[b], Mohammad Amanullah[a], Manfred Morari[b], Marco Mazzotti[a,*], Massimo Morbidelli[c]

[a] *ETH-Zürich, Institute of Process Engineering, Sonneggstrasse 3, 8092 Zürich, Switzerland*
[b] *ETH-Zürich, Automatic Control Laboratory, Physikstrasse* 3, 8092 *Zürich, Switzerland*
[c] *ETH-Zürich, Institute for Chemical and Bio-Engineering,* 8093 *Zürich, Switzerland*

Available online 15 July 2005

Abstract

The operation of simulated moving beds (SMBs) at their optimal operating conditions is difficult and not robust. Therefore, it is common practice to operate SMB units far from their economic optimum in order to tolerate uncertainties in the system and minimize the effect of disturbances. Recently, we have proposed an on-line optimization based SMB control scheme that allows to exploit the full economic potential of SMB technology. The goal of this work is two-fold. Firstly, to experimentally evaluate and demonstrate the capability of the controller to optimize and operate the SMB units, thus delivering the products with maximum productivity and minimum solvent consumption. Secondly, to show the suitability of the controller even using a minimum of system information, thus making the detailed isotherm measurements redundant and saving time in the separation design phase. This paper reports and discusses the first experimental implementation of the control concept on a high purity separation of nucleosides (uridine, guanosine) with an eight-column four-section SMB where the species to be separated are retained on the source 30RPC stationary phase according to a linear isotherm.

Keywords: Simulated moving bed chromatography; Online optimization; Optimizing control; Repetitive model predictive control

1. Introduction

The simulated moving bed (SMB) is a continuous chromatographic separation technique based on a solid/liquid countercurrent contact used for the separation of mixtures in two fractions. The continuous nature of the process as well as the higher productivity and lower solvent consumption compared to single column chromatography has led to increased interest of the fine chemical and pharmaceutical industry [1,2]. It has become a well established operation, especially for enantioseparations, but it is also attractive for bioseparations. The simulated moving bed is a separation technique, which can be applied at all scales from laboratory to production. This makes it a very convenient choice for the development of new drugs, where the time to market can be significantly reduced if SMB is used after symmetric synthesis.

The scheme of an SMB is shown in Fig. 1. The unit is divided into four sections by the inlet and outlet streams, i.e. the two product outlets extract and raffinate, and the feed and desorbent inlets. Each section consists of several fixed-bed chromatographic columns. Approximating a true countercurrent process (true moving bed, TMB), the SMB simulates the otherwise difficult movement of the solid phase by periodic switches of all inlet and outlet ports by one column position in the direction of the fluid flow. The separation itself takes place in Sections 2 and 3. Sections 1 and 4 are necessary to regenerate the solid and the liquid, respectively. Contrary to true countercurrent processes such as the TMB, SMB reaches a cyclic steady state where the internal concentration profiles move in the direction of the fluid flow and the outlet compositions change periodically in time [3].

* Corresponding author. Tel.: +41 1 632 2456; fax: +41 1 632 1141.
E-mail address: mazzotti@ipe.mavt.ethz.ch (M. Mazzotti).

0021-9673/$ – see front matter © 2005 Elsevier B.V. All rights reserved.
doi:10.1016/j.chroma.2005.04.101

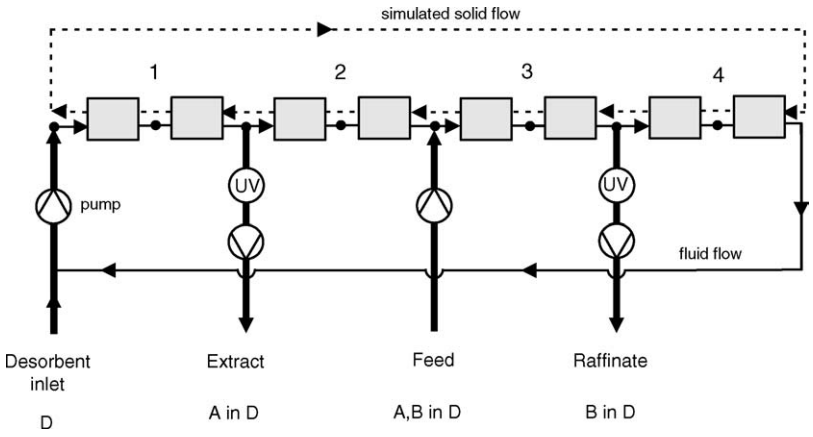

Fig. 1. Scheme of a simulated moving bed (SMB) unit including UV detectors for on-line concentration measurements in extract and raffinate.

Recently several new SMB schemes allowing for further improvements in the separation efficiency have been introduced [4–6]. Nevertheless, the operation of SMB units at their economic optimum is still an open issue. Close to the optimal point, the operation becomes less robust. In addition, uncertainties in terms of isotherm parameters, pump stability and calibration, temperature stability or aging of the columns make the operation at the optimum even more difficult. Therefore, it is common practice to choose a sub-optimal operating point in order to avoid off-spec production. Furthermore, proper off-line optimization requires a significant effort in system characterization such as a detailed isotherm measurement, which is rather time consuming.

Implementing a proper on-line feedback control scheme has the potential to allow for the operation of SMB units at their economic optimal conditions despite uncertainties and disturbances. However, the underlying characteristics of the SMB process, such as its non-steady-state, nonlinear and hybrid nature, make the control problem challenging. Several SMB control approaches have been proposed by other groups [7–12]. The common drawback of these approaches is the need for accurate data about the system. We have proposed a control strategy that integrates the on-line optimization and control of the SMB process, thus addressing the difficulties mentioned above [13–17]. A significant feature of the developed SMB control concept is that it is based on the linear adsorption isotherm and the overall average packing characteristic of the SMB unit only, regardless of the type of isotherm characterizing the separation system. This removes the necessity of detailed characterization of the columns and of the behavior of the mixture to be separated. This work presents and discusses the first experimental implementation of the developed concept for the high purity separation of nucleosides (uridine, guanosine) in a eight-column SMB unit.

2. On-line optimization based SMB control

To develop the proposed SMB control scheme, *repetitive model predictive control* (RMPC) was used [18,19]. The RMPC formulation is based on the assumption that possible model prediction errors and/or the effect of disturbances on the plant output are likely to repeat due to the periodic nature of the process, and therefore the information from the past

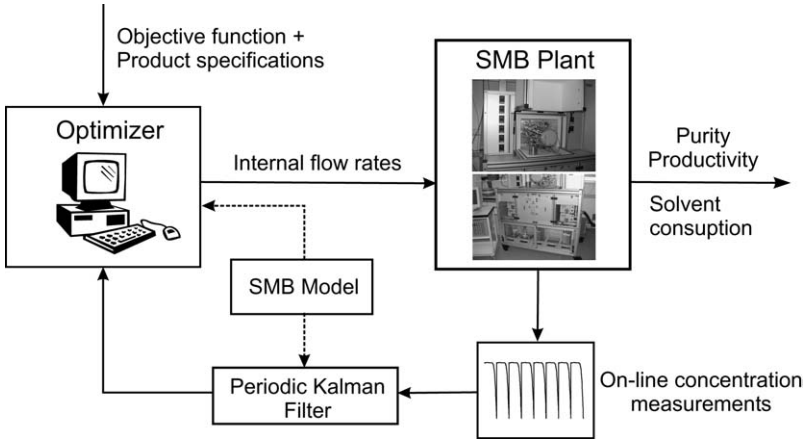

Fig. 2. Scheme of the optimization based control concept.

cycles can be used to correct the model errors in the future cycles. The applied control concept is shown schematically in Fig. 2 and a detailed description can be found in [13–15]. The core is an explicit, simplified SMB model. The internal flow rates in the four sections of the SMB and the concentration levels in the two outlet streams, extract and raffinate, are used as the manipulated and measured variables, respectively. The switching period t^* is defined at the beginning of the operation and kept constant. The goal is to optimize the performance of the plant in terms of productivity and solvent consumption on-line, while the purity of the products in extract and raffinate should be above a defined purity limit. The product concentrations are measured on-line by a suitable sensor system and are used as feedback information. The concentration measurements are used together with a periodic time-varying Kalman filter and the SMB model to estimate the current state of the plant. With this information the controller is then able, by using the SMB model, to predict the future evolution of the plant and to calculate an optimal plant input in terms of flow rates for the specified economical objective and product/process constraints. The controller is able to act on the plant by changing the flow rates in discrete time intervals. In our case an SMB cycle is divided into $N = 64$ time steps, i.e. eight time steps per switching interval in a eight-column SMB. The dynamics of an SMB plant is such that a flow rate change is not immediately effective, but some time is required for the concentration profiles to build up and for the outlet purities to change. Therefore, the controller predicts and optimizes the performance of the plant over a future time window of two cycles, i.e. the prediction horizon. The on-line optimization yields the optimal flow rate sequence to be implemented at the 64 time intervals of the first cycle, i.e. the control horizon, whereas only the calculated optimal flow rates for the first time step are indeed implemented. At the next time step, new feedback information becomes available and a new optimization problem is solved on the basis of the updated state of the process. Again only the flow rates corresponding to the following time step are implemented.

2.1. SMB model

A detailed SMB model is not suited for on-line optimization because of its nonlinear nature and excessive computational load. Therefore, a simplified model, i.e. a linear time-varying model of the process obtained via linearization of the equilibrium dispersive SMB model, is applied [14]. This model is simple enough for on-line computation and still captures the dynamics of the process sufficiently. The linear time-varying SMB model is obtained as briefly described below. A more detailed description of the modelling procedure can be found elsewhere [13,14].

The SMB process does not achieve a steady state in which all the process variables are constant in time, but it reaches a cyclic steady state, in fact the concentration profiles in the SMB propagate in the direction of the fluid flow and are shifted back at each port switch with respect to the inlet and outlet ports. In practice the true periodicity of the process is not a single switch, but the duration of an entire cycle, i.e. number of switches equal to the number of columns, because of possible small column to column differences. Therefore, we have defined N time steps per cycle ($N = 64$ in our case) and extracted N different internal profiles corresponding to the defined time instances, i.e. sample points. The nonlinear SMB model equations are linearized at each sample point using the corresponding cyclic steady-state concentration values and the flow rates in the four sections. Regardless of the specific adsorption isotherm, the SMB model is nonlinear because of the bilinear convective term where column flow rates and species concentration are multiplied. This procedure leads to the following linear time-varying state-space SMB model to be used in the control algorithm:

$$x_k(n+1) = A(n)x_k(n) + B(n)u_k(n),$$
$$y_k(n) = C(n)x_k(n) \quad \text{for} \quad n = 0, \ldots, N-1 \tag{1}$$

In the equation above, k is the cycle index and n is the time index within a cycle. The output vector y consists of the concentrations of the components A and B in both extract and raffinate, i.e. $c_A^{\mathrm{R}}(n)$, $c_B^{\mathrm{R}}(n)$, $c_A^{\mathrm{E}}(n)$ and $c_B^{\mathrm{E}}(n)$. The state vector x and the input vector u comprise the internal concentration values along the unit and the flow rates in the four sections, respectively. All variables are defined in terms of deviation variables. For instance, the state vector is defined as $x(n) = \mathbf{c}(n) - \mathbf{c}^{\mathrm{ref}}(n)$, where $\mathbf{c}^{\mathrm{ref}}$ is the reference internal concentration profile corresponding to time n used for the linearization of the nonlinear model equations. The transition from one cycle to the next can be written as:

$$x_{k+1}(0) = x_k(N) \tag{2}$$

This implies that the space composition profiles at the end of the current cycle k, are used as initial conditions for the next cycle $k+1$. The obtained time-varying linear model of the SMB process constitutes the basis for the on-line prediction and optimization of the process as described above. On the other hand, because the order of the obtained model is too high, it might lead to significant computational load for on-line applications. Hence, the order of the model is reduced by balanced model reduction technique. We refer to available literature for the details of the model reduction procedure [14].

2.2. Optimization problem

The aim of the developed control concept is to optimize the performance of the SMB plant. The controller should maximize the productivity PR (Eq. (3)) and minimize the desorbent requirement DR (Eq. (4)) while fulfilling constraints on a minimum product purity of extract and raffinate:

$$\mathrm{PR} = \frac{\text{amount separated per time}}{\text{volume solid phase}} = \frac{Q_{\mathrm{F}} c_{\mathrm{F}}}{n_{\mathrm{col}} V (1-\varepsilon^*)} \tag{3}$$

$$\mathrm{DR} = \frac{\text{desorbent consumption}}{\text{amount separated}} = \frac{(Q_\mathrm{D} + Q_\mathrm{F})\rho_\mathrm{D}}{Q_\mathrm{F} c_\mathrm{F}} \tag{4}$$

In the above equation, the density of the feed stream is assumed to be equal to the desorbent density, i.e. ρ_D, because of its high dilution. The plant equipment in terms of size and number of columns as well as column packing properties is given. A suitable switch time t^* and feed concentration c_F are fixed before the plant is started up. According to Eq. (3), the productivity can be maximized by maximizing the feed flow rate Q_F, i.e. the throughput. The desorbent requirement is minimized by minimizing the desorbent flow rate Q_D (see Eq. (4)).

Several constraints arising from technical limitations have to be fulfilled as well, e.g. constraints on the flow rates due to a maximum pressure drop limit. Here, the required product specifications are enforced by constraining the average purities over the prediction horizon, e.g. two cycles in our case, with a lower bound.

$$P_\mathrm{E}^\mathrm{ave} \geq P_\mathrm{E}^\mathrm{min} - s_1, \quad \text{where} \quad s_1 \geq 0 \tag{5}$$

$$P_\mathrm{R}^\mathrm{ave} \geq P_\mathrm{R}^\mathrm{min} - s_2, \quad \text{where} \quad s_2 \geq 0 \tag{6}$$

Slack variables, i.e. s_1 and s_2, are a standard method to eliminate the infeasibility problems that may occur during the on-line optimization. The feasibility of the purity constraints (Eqs. (5) and (6)) is guaranteed for sufficiently large values of s_1 and s_2. Excessive usage of slack variables is penalized in the cost function. The operating constraints due to hardware limitations such as maximum allowable flow rate related to the pressure drop limitations of the columns are also incorporated into the optimization problem as linear inequality constraints.

$$0 \leq Q_j \leq Q_j^\mathrm{max} \quad \text{for} \quad j = 1, \ldots, 4 \tag{7}$$

The cost function of the optimization problem is defined as minimizing the cumulative solvent consumption and maximizing the cumulative throughput over the control horizon, e.g. $n_\mathrm{c} = 1$ cycle in our case.

$$\min_{\mathbf{Q}^{n_\mathrm{c}}, \mathrm{s}} [\lambda_\mathrm{D} Q_\mathrm{D}^{n_\mathrm{c}} - \lambda_\mathrm{F} Q_\mathrm{F}^{n_\mathrm{c}} + \lambda_1 s_1 + \lambda_2 s_2] \tag{8}$$

In the expression above, $Q_\mathrm{D}^{n_\mathrm{c}}$ and $Q_\mathrm{F}^{n_\mathrm{c}}$ are the cumulative solvent consumption and throughput over the control horizon, respectively; λ_D and λ_F are the weights of the corresponding terms that are reflecting their importance in the operating objective. The vector $\mathbf{Q}^{n_\mathrm{c}}$ consists of the manipulated variables, i.e. internal flow rates, for the complete control horizon. The parameters λ_1, λ_2 are the weights of the corresponding slack variables in the cost function, which are kept large in order to punish their excessive use.

The linear cost function (Eq. (8)) together with the linear constraints (Eqs. (5)–(7)) constitutes a linear program (LP), i.e. with approximately 3000 constraints and 280 variables, to be solved on-line. ILOG CPLEX 7.0 is used as the commercial LP solver, and the maximum computation time to solve the LPs was 1.2 s on a PC with a 3 GHz processor. The effectiveness of this control approach has been demonstrated through extensive simulations in different cases (model/plant mismatch; disturbances), and for different linear and nonlinear adsorption isotherms [13–17].

3. Experimental

3.1. Materials and system characterization

The separation of the nucleosides uridine and guanosine (in the following also referred to as U and G, respectively), purchased from Sigma–Aldrich Chemie GmbH (Steinheim, Germany), on the reversed phase SOURCE™ 30RPC (Amersham Biosciences, AB, Uppsala, Sweden), was considered. This stationary phase is designed for fast, high performance preparative separations of bio-molecules such as proteins, peptides and oligonucleotides and has a matrix based on rigid, polystyrene/divinyl benzene 30 μm mono-sized beads. This material was slurry packed into nine standard stainless steel columns (10 cm × 1 cm) using a solvent mixture of 97% water and 3% ethanol with a flow rate of $Q = 40$ ml/min and 30 min packing time. The ethanol content of the solvent mixture used in the packing procedure is kept low on purpose, because operating the SMB unit with a solvent mixture that has a lower ethanol content than the one used for column packing might lead to shrinking of the packing material and might later change the column characteristics. As the first step of the system characterization, the adsorption behavior of the nucleosides was determined; their adsorption isotherms were found, i.e.:

$$q_\mathrm{i} = H_\mathrm{i} c_\mathrm{i} \quad (\mathrm{i} = \mathrm{G},\ \mathrm{U}) \tag{9}$$

The effect of the solvent composition on the adsorption behavior of uridine and guanosine has been investigated, as illustrated in Fig. 3. The Henry's constants H_i were calculated from the retention times $t_{\mathrm{R,i}}$ of dilute peaks and for ethanol

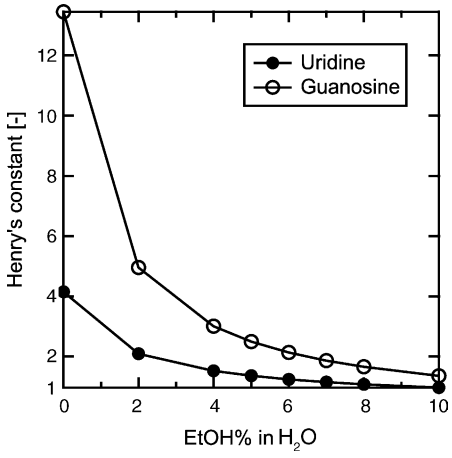

Fig. 3. Henry's constants of the nucleosides uridine and guanosine in mixtures of different ratios of ethanol and water at 22 °C.

Table 1
Column test with 5% ethanol in water at 22 °C; $c_U = c_G = 0.05$ g/l; $V_{inj} = 20$ μl

Column number	H_U	H_G	ε^*
1/spare column	1.274	2.168	0.367
2	1.327	2.293	0.377
3	1.351	2.334	0.373
4	1.344	2.324	0.374
5	1.349	2.328	0.375
6	1.332	2.301	0.378
7	1.328	2.295	0.375
8	1.330	2.268	0.372
9	1.321	2.248	0.374
Average (2–9)	1.335	2.299	0.375
σ (2–9)	0.011	0.030	0.0019

contents from 0 to 10%. The dead time due to the HPLC dead volume was subtracted first.

$$H_i = \frac{\varepsilon^*}{1-\varepsilon^*}\left(\frac{t_{R,i}-t_0}{t_0}\right) \quad (i = G,\ U) \tag{10}$$

Fig. 3 shows the Henry's constants of uridine and guanosine in mobile phases with different ethanol/water ratios at 22 °C. One can observe that both the selectivity, i.e. $S = H_G/H_U$, and the absolute values of the Henry's constants are increasing with decreasing ethanol content. The SMB operating conditions should be chosen in a way that the selectivity is high, i.e. the region of complete separation is large, so that the separation becomes easier and more robust, and the Henry's constants are small, so that one can use a low switch time t^* and increase the productivity [3]. On the other hand, the lower the switch time, the higher the internal flow rates; therefore, one needs to consider the pressure drop limitations when choosing the switch time. As a compromise, an ethanol content of 5% has been chosen for the experiments. The switch time was fixed at $t^* = 2$ min.

All the columns were tested by injecting a dilute pulse of uridine and guanosine (see Table 1). As a result of the tests, columns 2–9 were utilized in the SMB, whereas column 1, where the shape of the test pulse deviated slightly, was kept as a spare column. The overall void fraction, ε^*, of each column was determined by measuring the retention time of a pulse of pure water, which was assumed to be a non-retained species, according to the following equation, where the dead volume of the HPLC was properly accounted for:

$$t_0 = \frac{V\varepsilon^*}{Q} \tag{11}$$

In the equation above, t_0 is the retention time of the non-retained species; V the column volume and Q is the volumetric flow rate. Table 1 gives the overall void fraction of the columns. The average void fraction $\varepsilon^* = 0.375$ was used to design the separation. The effect of the fluid velocity on the column efficiency (see Van Deemter plot in Fig. 4) and on the pressure drop (see Eq. (15)) was determined. Column efficiency is expressed in terms of height equivalent to a theoretical plate (HETP), where the first term on the right hand side of Eq. (12) accounts for eddy diffusion and the second term accounts for mass transfer resistance:

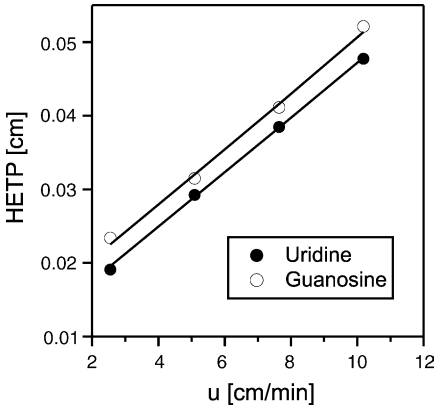

Fig. 4. HETP measurements (at 22 °C) and fitted line according to Eq. (14), where molecular diffusion could be neglected; ($D_{L,U} = 0.014$ cm^2/s and $D_{L,G} = 0.017$ cm^2/s at $u = 1$ cm/s, $a_p k_U = 318.8$ s^{-1}, $a_p k_G = 253.4$ s^{-1}).

$$\mathrm{HETP}_i = a_i + b_i u \quad (i = G,\ U) \tag{12}$$

The number of theoretical plates, $N_{p,i}$, and the HETP_i can be determined experimentally according to Eq. (13) by measuring the peak width at half height for different fluid velocities under dilute conditions, i.e. for symmetric peaks:

$$N_{p,i} = \frac{L}{\mathrm{HETP}_i} = 5.54\left(\frac{t_{R,i}}{w_i}\right)^2 \quad (i = G,\ U) \tag{13}$$

According to the lumped solid diffusion model of a chromatographic column under linear conditions, the following relationship applies [20]:

$$\mathrm{HETP}_i = \frac{L}{N_{p,i}} = \frac{2\varepsilon^* D_{L,i}}{u} + \frac{2u}{(1-\varepsilon^*)H_i a_p k_i} \times \left(\frac{(1-\varepsilon^*)H_i}{\varepsilon^* + (1-\varepsilon^*)H_i}\right)^2 \quad (i = G,\ U) \tag{14}$$

where $D_{L,i} = a_i u/2\varepsilon^*$. The model parameters for axial dispersion and mass transfer resistance can be estimated by fitting Eq. (14) to the experimental points, and are represented in the caption of Fig. 4, which shows the Van Deemter curves. The pressure drop of the columns is proportional to the velocity and the column length and was measured for an ethanol content of 5% to be:

$$\frac{\Delta p}{uL} = 0.0284\left(\frac{\text{bar min}}{\text{cm}^2}\right) \tag{15}$$

3.2. Laboratory SMB unit

The laboratory SMB unit comprises eight HPLC columns (10 cm × 1 cm i.d., particle diameter 30 μm) with two

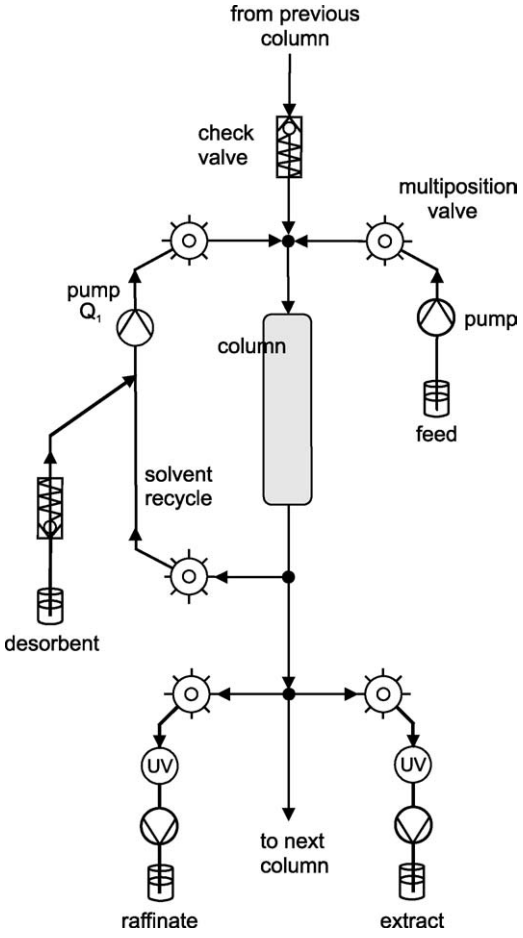

Fig. 5. Laboratory SMB setup: repetitive single column building block of the column loop.

columns in each section (2-2-2-2 configuration) and is located in a climate controlled room for isothermal operations. One of the eight modules of the plant setup is shown schematically in Fig. 5; this module is repeated eight times to constitute the SMB loop shown in Fig. 1. The unit is operated in closed loop mode, which means that the fluid phase is withdrawn at the end of Section 4 and directly recycled to Section 1. Three external streams, i.e. extract, feed and raffinate, as well as one internal stream, i.e. Q_1, are controlled by HPLC pumps (Jasco, PU-987). Five (12 + 1) port multiposition valves (Vici-Valco EMT-6-CSD12UW) implement the periodic port switching mechanism (see Fig. 5). The flow direction is determined by eight check valves (UPCHURCH, CV-3301), each located between two SMB columns as shown in Fig. 5. The outlet ports of each column and the inlet ports of the following one are located before and after the check valve, respectively, in order to establish the liquid flow in the unit and to avoid cross-contamination. The pressure after each column as well as the temperature in the unit are monitored. The plant is automated by a program using the software package LabView (National Instruments).

The dead volume in the experimental setup consists of the volume of piping, crossings and check valves. It can be neglected if the ratio between column volume and dead volume is large, which is not the case here but should be the case for most industrial SMB plants. As shown in Fig. 6, four different dead volume elements can be identified for each individual SMB column. These dead volume elements have been measured as $V_{d,\alpha} + V_{d,\beta} = 0.3705\,\text{ml}$, $V_{d,\gamma} = 0.01\,\text{ml}$ and $V_{d,\delta} = 0.041\,\text{ml}$. The dead volume per column in Sections 1–4 can be calculated from the number of columns in the section and the dead volume elements involved:

$$V_1^{\text{D}} = \frac{n_1^{\text{col}}(V_{d,\alpha} + V_{d,\beta} + V_{d,\gamma}) + (n_1^{\text{col}} - 1)V_{d,\delta}}{n_1^{\text{col}}} \tag{16}$$

$$V_2^{\text{D}} = \frac{V_{d,\delta} + n_2^{\text{col}}(V_{d,\alpha} + V_{d,\beta} + V_{d,\gamma} + V_{d,\delta})}{n_2^{\text{col}}} \tag{17}$$

$$V_3^{\text{D}} = \frac{n_3^{\text{col}}(V_{d,\alpha} + V_{d,\beta} + V_{d,\gamma}) + (n_3^{\text{col}} - 1)V_{d,\delta}}{n_3^{\text{col}}} \tag{18}$$

$$V_4^{\text{D}} = \frac{n_4^{\text{col}}(V_{d,\delta} + V_{d,\alpha} + V_{d,\beta}) + (n_4^{\text{col}} - 1)V_{d,\gamma}}{n_4^{\text{col}}} \tag{19}$$

For a 2-2-2-2 column configuration, as used in this work, the dead volumes per column were calculated to be: $V_1^{\text{D}} = V_3^{\text{D}} = 0.401\,\text{ml}$, $V_2^{\text{D}} = 0.442\,\text{ml}$ and $V_4^{\text{D}} = 0.4165\,\text{ml}$. Eq. (20) allows to calculate a dead volume correction for the flow rates Q_j yielding the following equation for the key operating parameters, i.e. the flow rate ratios, m_j [21]:

$$m_j = \frac{Q_j t^* - V\varepsilon^* - V_j^{\text{D}}}{V(1 - \varepsilon^*)} \quad (j = 1, \ldots, 4) \tag{20}$$

The laboratory SMB setup is arranged in the closed loop mode as illustrated in Fig. 5. There are different ways to close the loop in an SMB setup, where one straight forward method

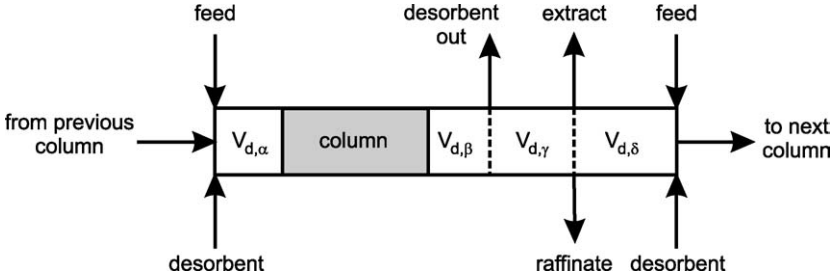

Fig. 6. Dead volume distribution for one column in the experimental SMB setup.

(adopted in this work) is to connect the multi-position valve at the "open loop desorbent outlet" directly to the pump controlling the internal flow rate Q_1 using a tee-connection to a bottle with fresh solvent (see Fig. 5). This way the solvent from Section 4 is directly recycled to Section 1 and fresh solvent makes up for the difference in solvent balance. By implementing the closed loop in this way, a dead volume between the desorbent outlet multi-position valve across the pump to the desorbent inlet multi-position valve is created. It is not part of the column loop and it does not influence V_4^{D}, but it introduces a short delay time for the profile to propagate from Sections 4–1, in case of incomplete regeneration in Section 4.

3.3. On-line monitoring

To implement a monitoring system suitable for on-line control, two sensors, one for each the extract and the raffinate outlets, are needed. Each sensor should be able to monitor continuously the nucleosides concentration in the binary mixture of the product streams. Since the concentrations of the two components can not be measured individually and a superimposed signal is to be expected, two different signals are needed from each sensor, e.g. UV absorbance at two different wave lengths, to calculate the concentration of each component. This yields a system of two equations (one for each signal) with two unknowns (concentration of the nucleosides), which can be solved for the concentrations c_{U} and c_{G}. Two multi-wavelength UV 2077 detectors (Jasco) were chosen as sensors. The two different signals can be obtained by simultaneous measurement at two different wavelengths, thus exploiting the difference in the UV spectra of uridine and guanosine (see Fig. 7). The feed concentrations of the SMB experiments were chosen low enough to allow the use of the UVs in the linear range of the calibration curve. For better measurement accuracy the four wavelengths $\lambda_1 = 212$ nm, $\lambda_2 = 224$ nm, $\lambda_3 = 244$ nm and $\lambda_4 = 280$ nm have been chosen, which leads to the following over-determined system of linear equations that is solved by least squares regression implemented in the LabView software package:

$$S_{\lambda_n} = k^{\mathrm{U}}_{\lambda_n} c_{\mathrm{U}} + k^{\mathrm{G}}_{\lambda_n} c_{\mathrm{G}}, \quad n = 1, \ldots, 4 \tag{21}$$

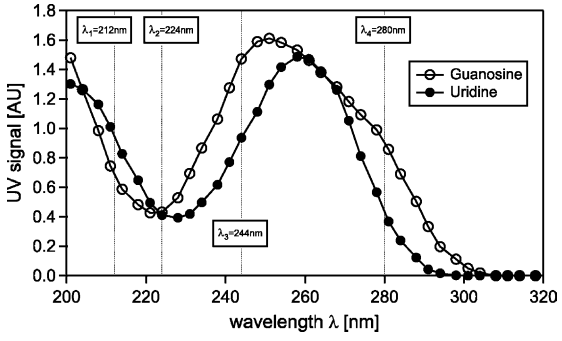

Fig. 7. UV spectra of guanosine and uridine measured with a multi-wavelength UV 2077 (Jasco); $c_{\mathrm{U}} = c_{\mathrm{G}} = 0.08$ g/l. For on-line monitoring, signals at the following wavelengths were used: $\lambda_1 = 212$ nm, $\lambda_2 = 224$ nm, $\lambda_3 = 244$ nm, $\lambda_4 = 280$ nm.

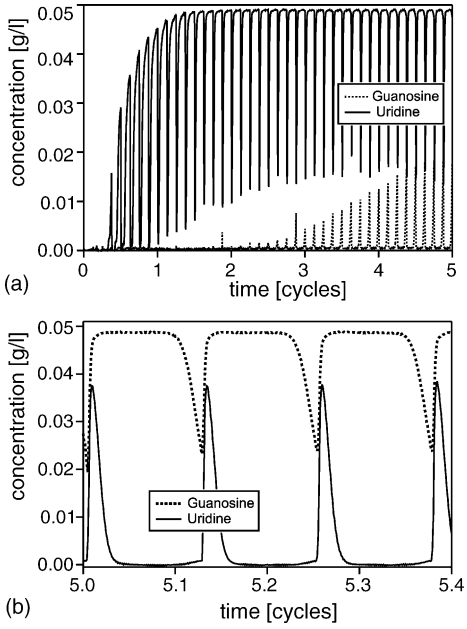

Fig. 8. On-line monitoring of the concentrations of guanosine and uridine (5% ethanol in water, $t^* = 2$ min, $m_1 = 2.276$, $m_2 = 1.263$, $m_3 = 2.294$, $m_4 = 1.298$) in (a) raffinate (plant startup) and (b) extract (close-up over three switch periods).

The UV detectors are positioned between the plant outlet multi-position valve of extract or raffinate and the corresponding pump, as shown in Figs. 1 and 5. At this position, the UVs are at the pressure of the plant. Hence they are equipped with high pressure flow cells for stable and reliable monitoring. The plant pressure is always below 20 bar, depending on the flow rates. Another option would have been to put the sensors after the outlet pump where the pressure is atmospheric. In this case the backmixing in the dead volume of the pump and of the tubings would influence the signal and introduce a time delay.

Fig. 8 shows the concentrations of uridine and guanosine calculated from the four monitored UV signals for the plant startup of the experiment described in Section 4.2.1. The plant startup is shown for the first five cycles for the raffinate in Fig. 8a and zoomed in on only three switching periods for the extract around cycle 5 in Fig. 8b. The dead volume between the multi-position valve at the plant outlet and the detector is almost negligible and a time delay of the measured signal of only 3 s (at a flow rate of $Q = 2$ ml/min) was calculated. This implies that there is almost no backmixing in the line between the plant and the detectors and, as can be observed from Fig. 8, the sensor system monitors the process dynamics very accurately. Small variations from column to column can not be completely avoided, which is evident from the pattern in Fig. 8a. The accuracy of the on-line monitoring system has been checked by off-line HPLC measurements for a lim-

ited number of SMB experiments and a statistical error of 0.5% on the resulting purity has been estimated. This error occurs as the sum of several influences such as calibration deviations at all four UV channels, slight pressure sensitivity of the sensor, drift of the UV signals, and concentration level of the compounds (signal-to-noise ratio). It has to be kept in mind that the achievable accuracy largely depends on the UV spectra of the two components to be separated and on the possibility to choose several wavelengths with a significant difference in measurement response. This implies that for a system with a larger difference in spectra a better accuracy can be achieved. The linearity range of the UV signal at different wave lengths is also a factor to be considered. For the system of guanosine and uridine the spectra are rather close (see Fig. 7), but a reasonable accuracy can still be obtained.

Table 2
SMB runs at different operating conditions and corresponding purities of raffinate and extract

Run	m_2	m_3	P_R	P_E
1	1.29	1.79	99.8	94.8
2	1.29	1.79	100.0	95.0
3	1.32	1.82	99.9	99.1
4	1.35	1.85	100.0	99.5
5	1.39	1.89	100.0	99.6
6	1.41	1.91	100.0	99.6
7	1.62	2.12	99.6	99.8
8	1.64	2.14	99.1	99.7
9	1.68	2.18	95.8	99.8
10	1.74	2.24	89.7	99.7
11	1.34	2.07	99.6	99.8
12	1.31	2.11	99.7	99.3
13	1.28	2.17	97.4	95.6

The flow rate ratios m_1 and m_4 are fixed as 2.891 and 0.880, respectively, and $t^* = 2$ min.

4. Results and discussion

4.1. SMB separation performance and temperature effects

Characterization of the columns and of the adsorption behavior of the mixture provide us with the information needed for the design of the SMB separation. This section is devoted to the experimental verification of the SMB separation performance before implementing the control scheme. Furthermore the temperature sensitivity of the system is an important issue to be clarified in order to assess the robustness of the SMB experiments. Therefore, the temperature effect on the adsorption behavior of each component, i.e. uridine and guanosine, is characterized by measuring their Henry's constants at different temperatures (see Fig. 9a). Fig. 9b illustrates the region of complete separation in the (m_2, m_3) operating plane for different temperatures, and gives an insight into the temperature sensitivity of the separation performance. The operating temperature for the SMB experiments is chosen as 23 °C in order to have the best temperature stability for the available climate control system.

The region of complete separation in the (m_2, m_3) operating parameter space at 23 °C was obtained using the data from single column Henry's constants measurements and is drawn with solid boundaries in Fig. 10. The validity of this region needs to be verified by SMB experiments. To this aim, SMB experiments with different operating conditions were run to steady state and the product purities were determined by HPLC measurements. All experiments were carried out at a constant switch time, i.e. $t^* = 2$ min, and fixed values of m_1 and m_4, i.e. $m_1 = 2.891$ and $m_4 = 0.880$, which guarantee complete regeneration in Sections 1 and 4, respectively. The dead volume of the plant was accounted for properly according to Eq. (20) [21]. Table 2 reports operating conditions and corresponding purities of raffinate and extract of the experimental runs. First, ten experiments were performed to verify the position of the complete separation region, whereas the last three were performed to identify the optimal operating conditions, i.e. those close to the vertex of the complete separation triangle. The reproducibility of the experiments was tested for one operating point ($m_2 = 1.286$, $m_3 = 1.789$) and a deviation of less than 0.22% in purity was found (see Table 2).

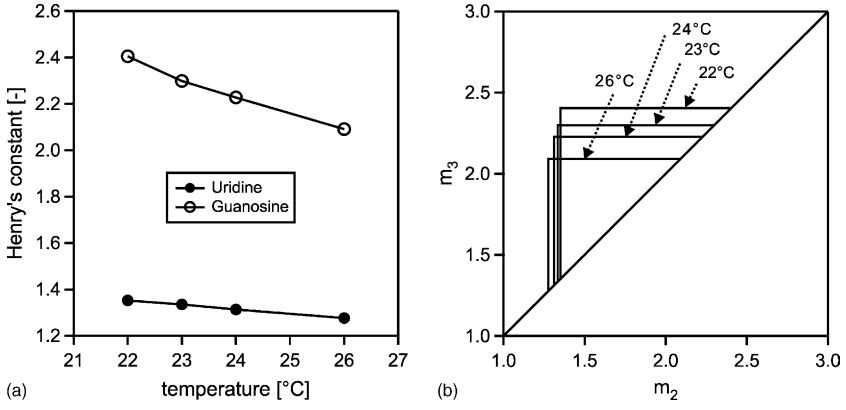

Fig. 9. (a) Temperature dependence of the Henry's constants of uridine and guanosine at 5% ethanol in water and (b) the resulting regions of complete separation in the (m_2, m_3) plane at different temperatures.

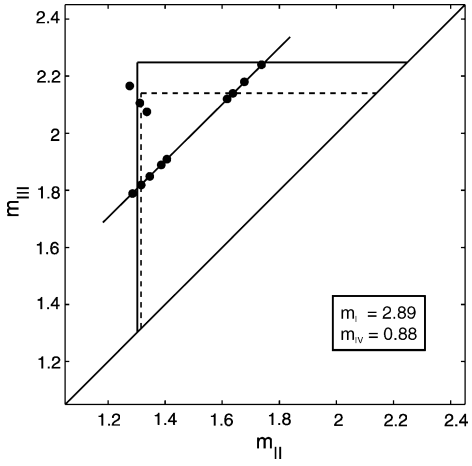

Fig. 10. Region of complete separation of guanosine and uridine at 23 °C for 5% ethanol in water. Solid line: separation region based on single column Henry's constants measurements; broken line: separation region estimated from SMB experiments. The operating points of those experiments are indicated, whereas $t^* = 2$ min, $m_1 = 2.89$ and $m_4 = 0.88$ were kept constant for all points.

Fig. 10 shows the position of the experimental points on the (m_2, m_3) operating plane, the obtained extract and raffinate purities are shown in Fig. 11. It can be observed that going along the line parallel to the diagonal with increasing m_2-values (see Fig. 10), the system behaves in the expected way, i.e. the extract purity increases and the raffinate purity decreases (see Fig. 11a). On the other hand, it is obvious from Fig. 10 and Fig. 11a that the triangular region of complete separation applied to the SMB unit is slightly shifted with respect to the one obtained using the measured Henry's constants (given in Fig. 10 with solid lines). According to the triangle theory, the operating points corresponding to the triangular region lead to 100% purity for both outlets. Here, the maximum achievable purity for both outlets was about 99.6%. Therefore, we have chosen 99% purity as the cutoff criterion and defined the borders of the experimental complete separation region accordingly. This is drawn in Fig. 10 with dashed boundaries.

The isotherm measurements were performed by controlling the HPLC column temperature, whereas the SMB runs were carried out by controlling the room temperature. Therefore, the mismatch between the complete separation regions determined by isotherm measurements and SMB experiments could be explained by a slightly higher temperature, e.g. ∼1 °C, inside the columns, whereas the room temperature was stable at about 23 °C. According to the triangle theory, the optimal operating conditions for an SMB separation are at the vertex of the complete separation region. Three more experiments were run (Run 11–13 in Table 2) and the vertex of the triangle region was located. The position of the operating points in the (m_2, m_3) operating plane is shown in Fig. 10, whereas Fig. 11b gives the corresponding product purities as a function of the corresponding m_2-values.

4.2. Controlled SMB separation of nucleosides

Our on-line optimization based SMB control concept has been implemented experimentally on the separation of nucleosides presented in the previous section. For all experiments given below, the switch time was fixed as $t^* = 2$ min, and the mobile phase was 5% ethanol in water. The operating temperature was chosen as 23 °C, but variations between 23 and 24 °C were to be expected due to the limited accuracy of the climate control in the room. The reduced-order time-varying linear SMB model used by the controller is obtained as described in Section 2.1 using $H_U = 1.303$, $H_G = 2.248$ and $\varepsilon^* = 0.375$. These are different from those obtained experimentally by running SMB experiments and used to draw the dashed triangle in Fig. 10, i.e. $H_U = 1.316$, $H_G = 2.140$ and $\varepsilon^* = 0.375$. This is done on purpose in order to introduce a plant/model mismatch and to challenge the robustness of the control concept.

4.2.1. Case of plant/model mismatch

Uncertainty in the retention behavior of the species is rather typical in SMB chromatography, e.g. due to measurement errors, temperature deviations, plant dead volume (see Section 4.1). Therefore, the SMB control concept should be

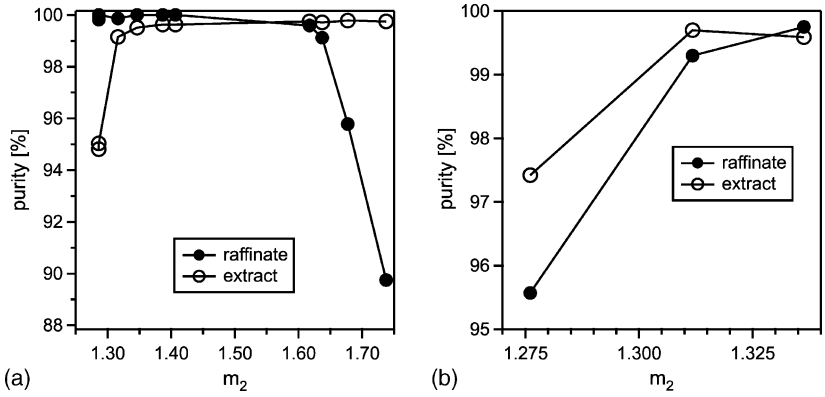

Fig. 11. Obtained steady state purities for the operating points shown in Fig. 10. (a) The points on the line parallel to the diagonal and (b) the points close to the vertex of the estimated separation region.

robust enough to yield good performance under such uncertainties. Hence, we have introduced a plant/model mismatch by developing the controller on the basis of isotherm parameters that are different from the real ones in the SMB plant. This result aims at demonstrating that the controller is able to fulfill the required product specifications and to operate the SMB unit at the optimal operating conditions despite uncertainties in the system behavior that are reflected in errors in the estimation of the model parameters.

The plant was started up without controller at an operating point above the complete separation region ($m_1 = 2.276, m_2 = 1.263, m_3 = 2.294, m_4 = 1.298$), thus leading to purities of $P_E = 90.4\%$ and $P_R = 91.4\%$ at cycle 8 as shown in Fig. 12. The low product purities are not only due to the wrong choices of the operating point in the (m_2, m_3) plane, but also due to the wrong values of m_1 and m_4 that lead to improper regeneration in Section 1 and 4.

The controller is switched on after cycle 8, to fulfill a specified purity requirement of $P^{min} \geq 99\%$ for both extract and raffinate. Recall that the primary task of the controller is the achievement and maintenance of the specified product purities despite uncertainties and disturbances, whereas the secondary task is the optimization of the separation performance in terms of productivity and solvent consumption. This objective is reflected by the cost function of the optimization problem (Eq. (8)) where proper weights are chosen, i.e. $\lambda_D = 4$, $\lambda_F = 18$, $\lambda_1 = 100$ and $\lambda_2 = 100$. Note that the weights are chosen by considering the relative magnitude of each term constituting the cost function rather than their absolute magnitude.

Fig. 12 shows the purities of extract and raffinate outlets measured by the on-line monitoring system and the production cost (F) throughout the entire operation, i.e. a duration of 54 h. The production cost (F) is defined according to the cost function of the optimization problem (Eq. (8)), but without the contribution of the slack variables:

$$F = \lambda_D Q_D^{ave} - \lambda_F Q_F^{ave} \tag{22}$$

Here Q_D^{ave} and Q_F^{ave} are the average solvent consumption and throughput over a cycle, respectively. One can see from Fig. 12 that once the controller is switched on, it adapts the operating conditions effectively and fulfills the specified product purities at the expense of the production cost, despite the plant/model mismatch. Following the fulfillment of the purity requirements, the production cost is then optimized. Note that if the products purities are above the specifications, there is room for the controller to optimize the economics of the process. The behavior of the controller reflecting this possibility can be clearly observed by looking at the dynamics of the product purities and of the production cost throughout the operation.

Fig. 13 shows how the controller changed the flow rate ratios in the four sections of the unit during the experiment in order to accomplish the given task. The resulting trajectory of the operating point with respect to the region of complete separation in the (m_2, m_3) plane and to the region of complete regeneration in the (m_4, m_1) plane, i.e. defined by $H_G \leq m_1$ and $H_U \geq m_4$, are illustrated in Fig. 14a and b, respectively. The regions with the dashed boundaries correspond to the real behavior in the SMB plant (at 23 °C), whereas the regions

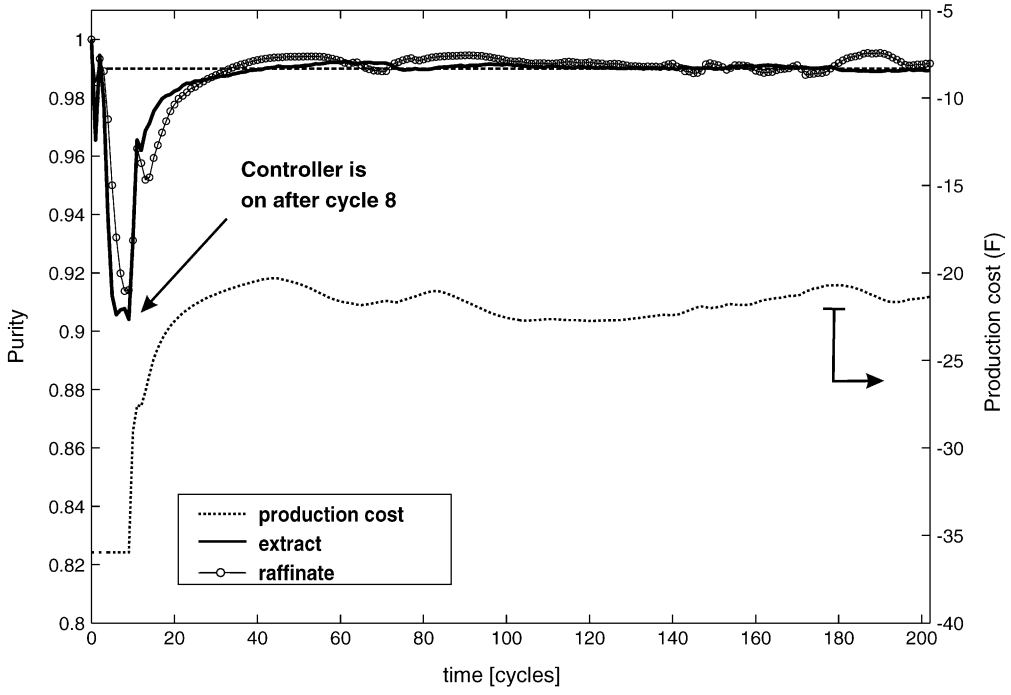

Fig. 12. Product purities of extract and raffinate and the production cost (F). The controller is switched on after cycle 8 in order to achieve a desired purity of minimum 99% for both products.

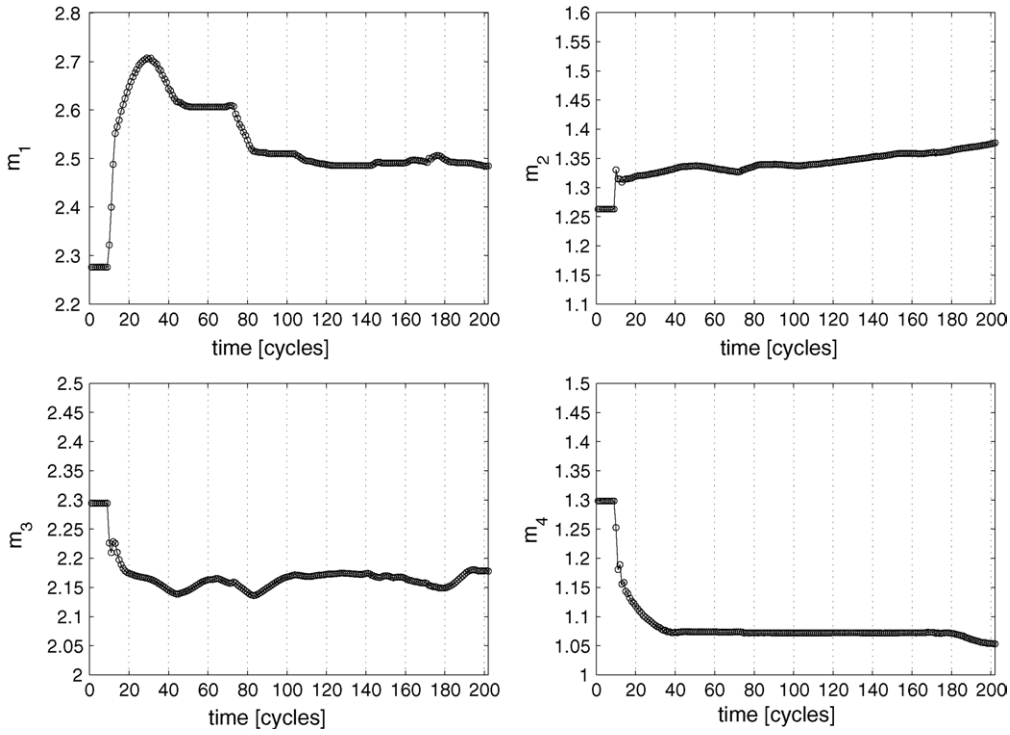

Fig. 13. Controller action throughout the operation in terms of flow rate ratios (m_j) that are calculated by average internal flow rates over one cycle.

with the solid boundaries are calculated based on the isotherm parameters used by the controller. One can see that after the controller is activated, i.e. after cycle 8, the operating point in the (m_2, m_3) plane is moved down towards the region of complete separation of the plant (see Fig. 14a). Moreover, m_1 and m_4 are changed so as the operating point is moved further inside the region of complete regeneration in order to overcome the regeneration problem (see Fig. 14b). Note that the SMB unit is operated close to the vertex of the triangular region (see Fig. 14a), which corresponds to the optimal operating conditions according to triangle theory [3].

This result demonstrates that the controller does not need to rely on accurate system parameters to achieve the product specifications and to optimize the economics of the process.

4.2.2. *Case of disturbance in the SMB operation*

As stated above, the task of the controller is to assure the product quality and to operate the SMB unit despite uncertainties and disturbances. Having shown the robustness of the control scheme against uncertainties, here we aim at assessing the performance of the controller when the SMB plant is

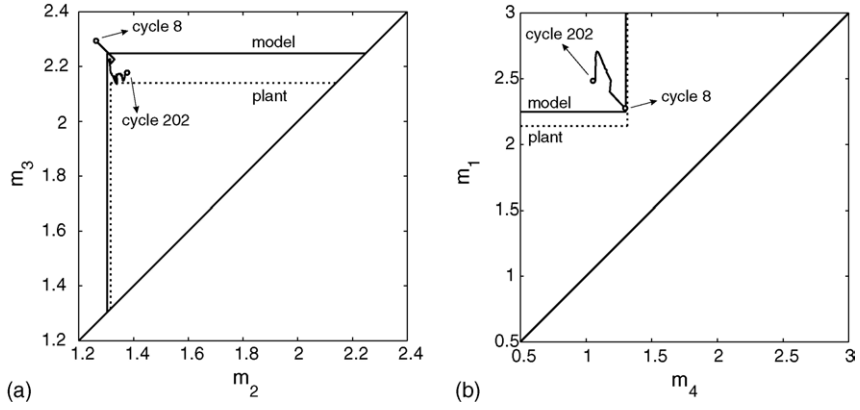

Fig. 14. (a) Trajectory of the operating point on the (m_2, m_3) plane with respect to the region of complete separation. (b) Trajectory of the operating point on the on the (m_4, m_1) plane with respect to the region of complete regeneration. The regions given by dotted line are valid for the SMB plant, whereas the ones with solid line are based on the isotherm information that is used to obtain the SMB model of the control scheme.

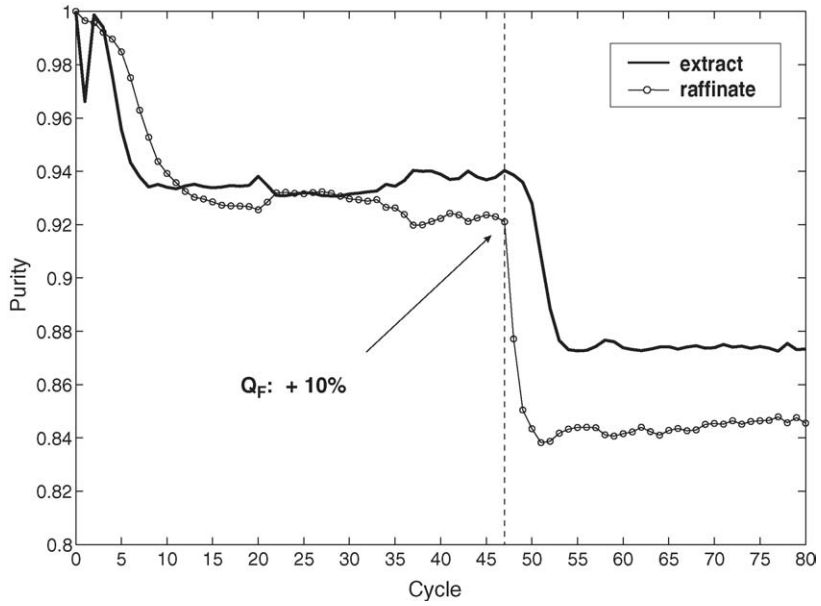

Fig. 15. Product purities of extract and raffinate, not controlled, same start up conditions as above ($m_1 = 2.276$, $m_2 = 1.263$, $m_3 = 2.294$, $m_4 = 1.298$, $t^* = 2$ min). A 10% increase of the feed flow rate is introduced as a disturbance after cycle 47.

subjected to disturbances. The most common SMB configurations require four to five pumps and operational problems due to malfunctioning of the pumps are familiar to SMB practitioners. Therefore, in this second test case we considered a situation in which the feed pump starts to deliver 10% more flow from a certain point on for the rest of the operation.

Before investigating the behavior of the controller under such circumstances, it is important to quantify the effect of such a disturbance on an SMB plant operated without any control scheme, so that the control performance can be appreciated. To this aim, the SMB plant is started up under the same conditions as in the previous case (see Section 4.2.1)

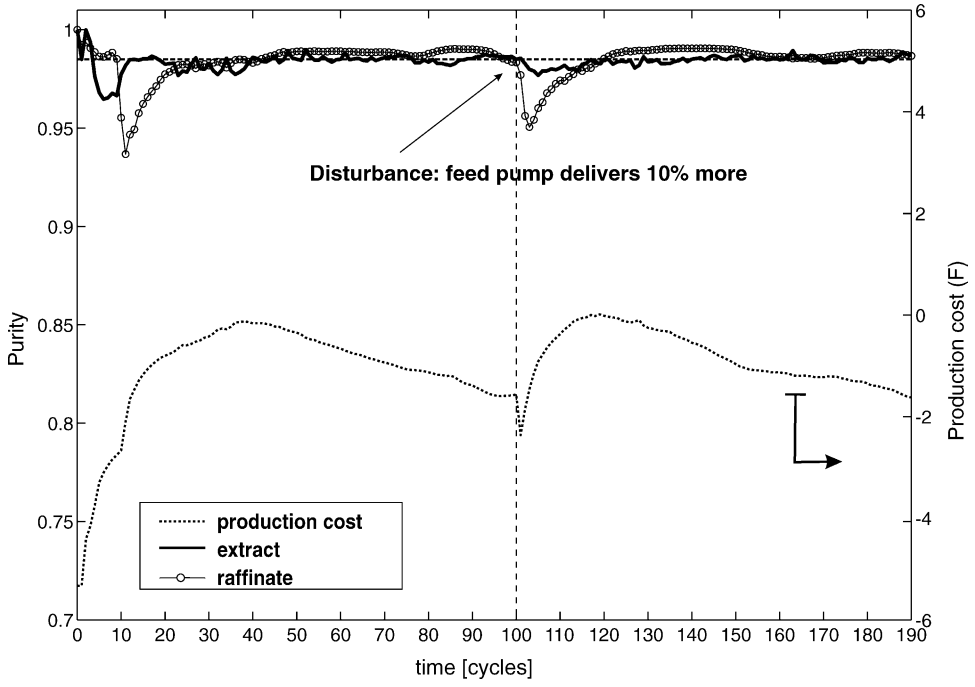

Fig. 16. Product purities of extract and raffinate and production cost (F). The controller is switched on after cycle 1 in order to achieve a desired purity of above 98.5% for both products. The disturbance on the feed pump (unknown to the controller) is implemented at the end of cycle 100 and feed pump starts to deliver 10% more than it should do.

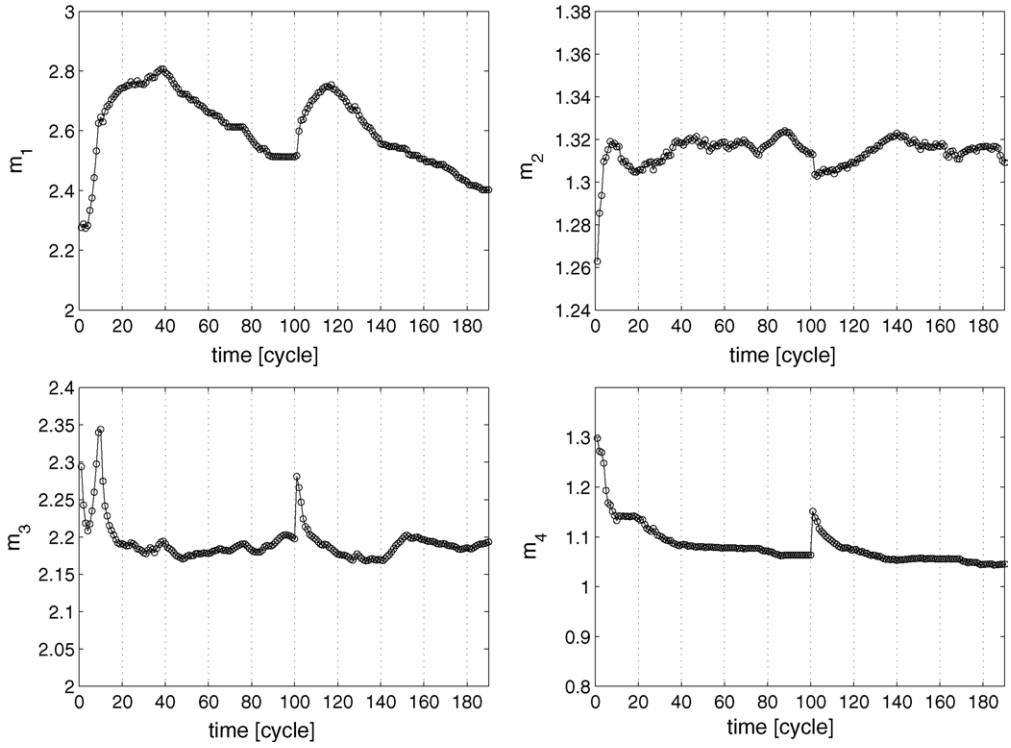

Fig. 17. Controller action throughout the operation in terms of flow rate ratios (m_j) that are calculated by average internal flow rates over one cycle. The disturbance on the feed pump (unknown to the controller) is implemented at the end of cycle 100 and feed pump starts to deliver 10% more than it should do, which causes the discontinuity in m_3 and m_4.

and run until it reaches steady state. The feed flow rate is increased by 10% after cycle 47 in order to illustrate the effect of such a disturbance on the separation performance of an uncontrolled SMB unit. Fig. 15 gives the corresponding plant response in terms of product purities. It can be seen that the start up operating conditions lead to a purity of about 94% and 92% for extract and raffinate, respectively, whereas the change in the feed flow rate results in a 7% decrease in the purity of both outlets. Note that the extract and raffinate purities are fluctuating slightly even at steady state conditions. This is probably due to temperature variations in the system and possibly also due to pulsations of the pumps. This actually indicates that the system is already subject to disturbances that are hard to avoid completely.

The controlled SMB operation is started up under the same initial conditions as in the case illustrated in Fig. 15 and the controller is switched on after the first cycle. The specified minimum purity requirement is defined as $P^{\min} \geq 98.5\%$ for both extract and raffinate. This constraint is fulfilled after about 25 cycles following the start up (see Fig. 16). The disturbance, which is of course unknown to the controller, is implemented after cycle 100. The feed pump delivers 10% more flow for the rest of the operation. It can be observed from Fig. 16 that the controller rejects the disturbance and recovers the required outlet purities within 20 cycles, at the expense of the production cost that increases. Once the product specifications are achieved, the cost is improved and then optimized.

Fig. 17 illustrates the controller action in terms of flow rate ratios, m_j, throughout the operation. The implemented disturbance affects directly the flow rates in Sections 3 and 4, by increasing them. One can see that the controller counteracts and compensates for the consequences of the increased feed flow rate. It is worth mentioning that the controller operates the plant very close to the vertex of the complete separation region in the (m_2, m_3) plane both before and after the disturbance.

As a final remark, this operation is carried out by using slightly different weights in the cost function of the optimization problem with respect to the test case in Section 4.2.1, i.e. $\lambda_D = 2$, $\lambda_F = 4$, $\lambda_1 = 100$ and $\lambda_2 = 100$. It can be observed that the values of the weights do not have a significant influence on the controller performance, provided there is a clear difference in the relative magnitude of the terms constituting the cost function, i.e. $\lambda_D\, Q_D^{n_c}$ and $\lambda_F\, Q_F^{n_c}$.

This result demonstrates that the controller can minimize the off-spec production, assure the product quality and optimize the performance of the plant despite major disturbances in the SMB operation.

5. Conclusions

In this work, we have presented the experimental implementation of an optimizing controller for SMB units that has several remarkable features. The controller is based on

a simplified model of the SMB unit, and does not require that this model is very accurate, i.e. it is able to cope with significant uncertainties in the model parameters. It relies on feedback information from the plant in terms of composition, hence purity, of extract and raffinate. In earlier works, we had demonstrated the effectiveness of the controller when applied to a virtual SMB plant, in the case of systems characterized by both linear and nonlinear isotherms. Here, we have shown that the controller works indeed also on a real SMB plant, which in this case is a eight-column SMB used for the separation of the nucleosides uridine and guanosine. The compounds to be separated exhibit linear adsorption behavior, and on-line information about product composition has been obtained by using data about UV absorbance at different wave lengths. These results open up rather promising perspectives in SMB chromatography, namely the possibility of reducing to a minimum the time for system characterization before starting a preparative SMB separation. This looks particularly attractive for chiral systems and for multicomponent separations where adsorption characterization may be very time consuming.

6. Nomenclature

a_p	specific surface of the adsorbent particles (cm^{-1})
A, B, C	state space model matrices
c_i	concentration of species i (g/l)
F	production cost function (ml/min)
H_i	Henry's constant of species i
$HETP_i$	height equivalent of a theoretical plate (cm)
k_i	mass transfer coefficient of component i (cm/s)
k_λ	UV calibration factor (AU l/g)
m_j	flow rate ratio in section j
N	number of time steps per cycle
N_p	number of theoretical plates
n_j^{col}	number of columns in section j
n_c	control horizon (cycles)
P	purity
q_i	adsorbed phase concentration of species i (g/l)
Q_j	volumetric fluid flow rate in section j (ml/min)
s	slack variable
S	UV signal (AU)
t^*	switch time (min)
t_0	retention time of non-retained species (min)
$t_{R,i}$	retention time of component i (min)
u	input vector of superficial velocities
V	column volume (ml)
V_j^D	dead volume per column in section j (ml)
V_d	dead volume element (ml)
w_i	peak width at half height (min)
x	state vector
y	output concentration vector

Greek letters

ε^*	void fraction
λ_D, λ_F, λ_1, λ_2	weighting factor in cost function
λ	wave length (nm)

Subscripts and superscripts

ave	average
A, B	components
D	desorbent
E	extract
F	feed
G	guanosine
i	component index
j	section index ($j = 1, \ldots, 4$)
k	cycle index
max	maximum
min	minimum
n	time step index within a cycle ($n = 0, \ldots, N-1$)
n_c	over the control horizon
R	raffinate
ref	reference
U	uridine

References

[1] M. Juza, M. Mazzotti, M. Morbidelli, Simulated moving-bed chromatography and its application to chirotechnology, Trends Biotechnol. 18 (2000) 108.

[2] R.M. Nicoud, Simulated moving bed: some possible applications of biotechnology, in: G. Subramanian (Ed.), Bioseparation and Bioprocessing, Wiley-VCH, New York, 1998.

[3] M. Mazzotti, G. Storti, M. Morbidelli, Optimal operation of simulated moving bed units for nonlinear chromatographic separations, J. Chromatogr. A 769 (1997) 3.

[4] O. Ludemann-Hombourger, R.M. Nicoud, M. Bailly, The VARICOL process: a new multicolumn continuous chromatographic process, Sep. Sci. Technol. 35 (2000) 1829.

[5] Z. Zhang, M. Mazzotti, M. Morbidelli, Experimental assessment of PowerFeed chromatography, AIChE J. 50 (2004) 625.

[6] H. Schramm, M. Kaspereit, A. Kienle, A. Seidel-Morgenstern, Simulated moving bed process with cyclic modulation of the feed concentration, J. Chromatogr. A 1006 (2003) 77.

[7] E. Kloppenburg, E.D. Gilles, Automatic control of the simulated moving bed process for C_8 aromatics separation using asymptotically exact input/output-linearization, J. Process Control 9 (1999) 41.

[8] K.U. Klatt, F. Hanisch, G. Dünnebier, S. Engell, Model-based optimization and control of chromatographic processes, Comput. Chem. Eng. 24 (2000) 1119.

[9] K.U. Klatt, F. Hanisch, G. Dünnebier, Model-based control of a simulated moving bed chromatographic process for the separation of fructose and glucose, J. Process Control 12 (2002) 203.

[10] C. Wang, K.U. Klatt, G. Dünnebier, S. Engell, F. Hanisch, Neural network-based identification of SMB chromatographic processes, Control Eng. Practice 11 (8) (2003) 949.

[11] H. Schramm, S. Grüner, A. Kienle, Optimal operation of simulated moving bed chromatographic processes by means of simple feedback control, J. Chromatogr. A 1006 (1–2) (2003) 3.

[12] Song, I.-H. and Rhee, H.-K. and Mazzotti, M., Identification and predictive control of simulated moving bed process, in: Proceedings of the Third Pacific Basin Conference on Adsorption Science and Technology, Kyongju, Korea, 2003.

[13] S. Abel, G. Erdem, M. Mazzotti, M. Morari, M. Morbidelli, Optimizing control of simulated moving beds—linear isotherm, J. Chromatogr. A 1033 (2) (2004) 229.

[14] G. Erdem, S. Abel, M. Morari, M. Mazzotti, M. Morbidelli, J.H. Lee, Automatic control of simulated moving beds, Ind. Eng. Chem. Res. 43 (2) (2004) 405.
[15] G. Erdem, S. Abel, M. Morari, M. Mazzotti, M. Morbidelli, Automatic control of simulated moving beds. II. Nonlinear isotherm, Ind. Eng. Chem. Res. 43 (14) (2004) 3895.
[16] G. Erdem, S. Abel, M. Morari, M. Mazzotti, M. Morbidelli, Online optimization based feedback control of simulated moving bed chromatographic units, Chem. Biochem. Eng. Quart. 18 (4) (2004) 319.
[17] G. Erdem, S. Abel, M. AmanUllah, M. Morari, M. Mazzotti, M. Morbidelli, Automatic control of simulated moving beds—experimental verification, Adsorption, in press.
[18] S. Natarajan, J.H. Lee, Repetitive model predictive control applied to a simulated moving bed chromatography system, Comput. Chem. Eng. 24 (2000) 1127.
[19] J.H. Lee, S. Natarajan, K.S. Lee, A model-based predictive control approach to repetitive control of continuous processes with periodic operations, J. Process Control 11 (2001) 195.
[20] C. Migliorini, A. Gentilini, M. Mazzotti, M. Morbidelli, Design of simulated moving bed units under non-ideal conditions, Ind. Eng. Chem. Res. 38 (1999) 2400.
[21] C. Migliorini, M. Mazzotti, M. Morbidelli, Simulated moving bed units with extracolumn dead volume, AIChE J. 45 (1999) 1411.